



Spreading of perturbations in myosin group kinetics along actin filaments

Zsombor Balassy^{a,b,c}, Anne-Marie Lauzon^{a,b,c,d}, and Lennart Hilbert^{a,c,e,f,g,h,i,1}

^aDepartment of Physiology, McGill University, Montreal, QC H3G 1Y6, Canada; ^bDepartment of Biomedical Engineering, McGill University, Montreal, QC H3A 2B4, Canada; ^cMeakins-Christie Laboratories, Research Institute of the McGill University Health Centre, Montreal, QC H4A 3J1, Canada; ^dDepartment of Medicine, McGill University, Montreal, QC H4A 3J1, Canada; ^eInstitute of Toxicology and Genetics, Karlsruhe Institute of Technology, 76021 Karlsruhe, Germany; ^fZoological Institute, Systems Biology and Bioinformatics, Karlsruhe Institute of Technology, 76131 Karlsruhe, Germany; ^gCenter for Systems Biology, 01307 Dresden, Germany; ^hMax Planck Institute for the Physics of Complex Systems, 01187 Dresden, Germany; and ⁱMax Planck Institute of Molecular Cell Biology and Genetics, 01307 Dresden, Germany

Edited by David A. Weitz, Harvard University, Cambridge, MA, and approved July 22, 2019 (received for review March 10, 2019)

Global changes in the state of spatially distributed systems can often be traced back to perturbations that arise locally. Whether such local perturbations grow into global changes depends on the system geometry and the spatial spreading of these perturbations. Here, we investigate how different spreading behaviors of local perturbations determine their global impact in 1-dimensional systems of different size. Specifically, we assessed sliding arrest events in in vitro motility assays where myosins propel actin, and simulated the underlying mechanochemistry of myosins that bind along the actin filament. We observed spontaneous sliding arrest events that occurred more frequently for shorter actin filaments. This observation could be explained by spontaneous local arrest of myosin kinetics that stabilizes once it spreads throughout an entire actin filament. When we introduced intermediate concentrations of the actin cross-linker filamin, longer actin was arrested more frequently. This observation was reproduced by simulations where filamin binding induces persistent local arrest of myosin kinetics, which subsequently spreads throughout the actin filament. A spin chain model with nearest-neighbor coupling reproduced key features of our experiments and simulations, thus extending to other linear systems with nearest-neighbor coupling the following conclusions: 1) perturbations that are persistent only once they spread throughout the system are more effective in smaller systems, and 2) perturbations that are persistent upon their establishment are more effective in larger systems. Beyond these general conclusions, our work also provides a theoretical model of collective myosin kinetics with a finite range of mechanical coupling along the actin filament.

actin–myosin interaction | smooth muscle | filamin | molecular motor cooperativity | dynamical systems

Changes in spatially distributed systems are often the consequence of local events that spread to global extent. Examples include nucleation of phases of matter (1), traffic jams (2), or sociopolitical phenomena (3). The global impact of local events depends both on the spreading behavior of such events, as seen for disease outbreak (4), and the system's overall geometry, as seen in obstacle-induced symmetry breaking in reconstituted heart tissue (5). A fundamental question that arises is how the spatial spreading of local events and overall system geometry together determine whether system-wide changes occur.

We wanted to address this question in an example system. Ideally, such a system would undergo frequent and obvious changes in system-wide behavior, which result from well-understood and experimentally adjustable local interactions, and exhibit a range of system geometries. These criteria are fulfilled by the in vitro motility assay (6), where actin filaments of different lengths are propelled by surface-bound groups of myosin molecular motors (Fig. 1A). Individual myosin motors interact with equidistant binding sites (7) along the actin filament (Fig. 1B). The resulting unidirectional motion of the actin filament is characterized by periods of arrest and continuous forward sliding (Fig. 1C). With

increasing filament length, filaments are increasingly biased into the sliding state (Fig. 1C). Previous theoretical work explained the observed periods of arrest and sliding by 2 group kinetic states that emerge by mechanical coupling of myosins via the actin filament (8) (Fig. 1D). Specifically, the group kinetic states corresponding to actin arrest or sliding are molecularly characterized by persistent binding at all myosin binding sites or a balanced mixture of bound and unbound binding sites, respectively. Furthermore, it was shown that experimentally induced changes in single myosin mechanochemistry proliferate into altered actin sliding patterns (9, 10). Last, statistical distributions of actin sliding velocities for different lengths of filaments can be extracted using automated actin tracking software (9). Taken together, the in vitro motility assay is a good example system to study how locally coupled, experimentally modifiable, and theoretically well-understood myosin kinetics controls the bistable switching in the sliding of actin filaments of different length.

Here, we used in vitro motility assays of myosin purified from phasic smooth muscle and performed simulations with single-molecule resolution to investigate how different types of local molecular mechanical perturbations impact the sliding of actin filaments of different length. First, we investigated spontaneous kinetic arrest. Combining experiments and simulations, we found that spontaneous arrest initiates locally, involving a few myosins at close-by positions on the actin filament. Such arrest becomes long-term stable only when it affects further myosins and in this

Significance

The emergence of spatially distributed phenomena, such as traffic jams or disease outbreaks, results from spreading of local events to larger scale. We investigated spreading of local events in the simplified situation of a 1-dimensional system. In particular, we addressed perturbations in the mechanochemistry of groups of myosin molecular motors that propel linear actin filaments. Using in vitro experiments and simulations, we conclude that perturbations spread along filaments by local mechanical coupling; the kinetic stability of a given perturbation and actin length together determine the likelihood that a perturbation has system-wide impact. We also generalized these findings to a spin chain model with nearest-neighbor coupling, meaning that they should also apply in other systems with local coupling and linear geometry.

Author contributions: Z.B., A.-M.L., and L.H. designed research; Z.B. and L.H. performed research; Z.B. and L.H. analyzed data; and Z.B., A.-M.L., and L.H. wrote the paper.

The authors declare no conflict of interest.

This article is a PNAS Direct Submission.

Published under the PNAS license.

¹To whom correspondence may be addressed. Email: lennart.hilbert@kit.edu.

This article contains supporting information online at www.pnas.org/lookup/suppl/doi:10.1073/pnas.1904164116/-DCSupplemental.

Published online August 12, 2019.

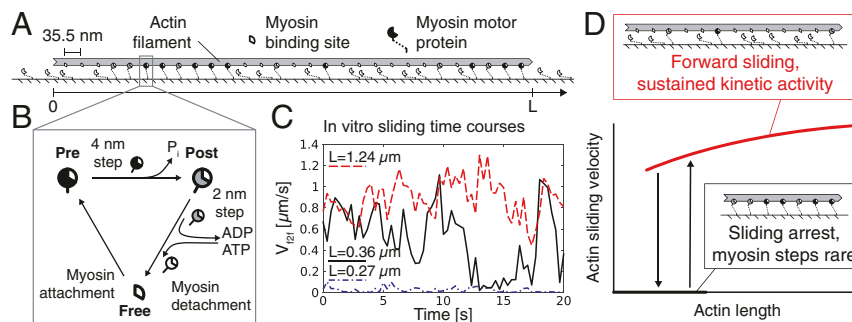


Fig. 1. In vitro propulsion of single actin filaments by muscle myosin groups exhibits an actin length-dependent stop-and-go pattern. (A) In our motility assays, purified smooth muscle myosin motors were immobilized on a glass surface to mediate the unidirectional sliding of fluorescently labeled actin filaments. Myosins can bind to actin every 35.5 nm (7). Myosin binding is oriented with respect to the filament sliding direction. (B) Individual myosin binding sites go through unidirectional kinetic cycles consisting of 3 main states (8, 10): unoccupied (Free), pre-power stroke (Pre), and post-power stroke (Post). The transitions occur by load-independent myosin attachment and load-dependent mechanochemical transitions. (C) Three example time courses showing instantaneous sliding velocities ("frame-to-frame velocities," V_{slid}) for actin filaments of different length (L). As previous work has shown, actin sliding exhibits L -dependent, bistable switching (8, 10); the shortest actin filaments (diffraction-limited, $L \lesssim 0.3 \mu\text{m}$) are permanently arrested; slightly longer actin filaments exhibit bistable switching between sliding and arrest; for $L \geq 1 \mu\text{m}$, actin slides continuously. (D) Previous work explained how the mechanical coupling of individual myosin motors via the actin filament results in 2 emergent states in myosin groups, which underlie the actin stop-and-go motion (8, 10). For short actin, myosins bind to actin but fail to effectively undergo mechanical steps due to the mechanical hindrance exerted by other bound myosins. For long actin, myosins bind, execute their mechanical steps, and rapidly unbind again, leading to sustained forward sliding of the actin filament. For actin of intermediate length, alternation between the 2 emergent states results in a stop-and-go sliding pattern.

way spreads to reach both ends of the filament. Before the arrest has reached both filament ends, it is readily dissolved. Spontaneous arrest therefore more frequently leads to arrest of shorter actin filaments. To generalize this finding, we implemented an abstract model consisting of a linear spin chain with nearest-neighbor coupling. In this abstract model, spontaneous arrest also more frequently spreads to global arrest in shorter chains. Second, we introduced the smooth muscle cross-linker filamin A, which establishes relatively stable actin-surface links throughout the length of actin (11–13). Again combining experiments and simulations, we found that persistent local kinetic arrest is established once such a link occurs, and subsequently spreads to arrest myosin kinetics globally. Because longer actin provides more possibilities for the occurrence of such cross-links, longer actin filaments are more strongly affected. Again, we could generalize this finding using the abstract spin chain model. Taken together, we found that the probability that local perturbations result in global arrest changes differently with system length, depending on whether these perturbations become stable immediately or only once they have spread to span the entire system.

Results

Spontaneous Kinetic Arrest Stabilizes after Spreading through the Entire Actin Filament. To understand how local interactions between myosins result in the arrest of the entire actin filament, we developed a spatially resolved theoretical model of myosin group kinetics. Several other models for the mechanochemistry of myosin groups have been developed. One widely used model posits that myosins independently interact with actin, and that actin slides at maximal velocity (v_{max}) whenever at least 1 myosin is attached (14). While this model is convincing in its simplicity, it cannot explain the observation that individual myosin kinetics is accelerated when myosins propel actin filaments as a group (15, 16). Such accelerated myosin kinetics emerges naturally in a model where myosin detachment is accelerated by mechanical forces imposed by other myosin molecules (17, 18). In particular, the mechanical force is communicated via the actin filament as an infinitely stiff mechanical link, is calculated prior to the mechanical step, and is assumed to modify the rate of the detachment step. The same model also explained mechanical oscillations in several seminal studies, where myosin groups work against elastic external loads (19–24). Further studies revealed

complex dynamics for externally unloaded actin filaments that are propelled by skeletal muscle myosin, smooth muscle myosin, or myosin VI (8, 9, 25). Specifically, intermediate-size groups of myosins exhibit a coordinated stop-and-go behavior; only sufficiently large groups attain uninterrupted kinetic activity (Fig. 1 C and D). To reproduce these observations, the previous model had to be extended to 1) consider changes in mechanical work associated with a given mechanochemical transition, and 2) explicitly consider the load-dependent kinetics of phosphate release during the main power stroke [cf. *Methods Summary* and previous work (8, 26–28)]. This extended model, however, predicts that actin sliding velocity increases linearly with actin length (SI Appendix, Fig. S1); in experiments, the actin sliding velocity saturates at a characteristic level, typically referred to as v_{max} . We suspected that this incorrect model behavior resulted from the unrealistic, although widely used, assumption that actin is an infinitely stiff mechanical link among simultaneously attached myosins. When we instead assumed that the mechanical coupling strength decays with distance along the actin filament, we recovered a more realistic saturation of sliding velocity with increasing actin length (SI Appendix, Fig. S1). Note that the specific function used to model the decay did not influence this result (SI Appendix, Fig. S1), and that the decay length of $\approx 300 \text{ nm}$ was in good agreement with a lower bound of $\approx 140 \text{ nm}$ estimated from previous stiffness measurements (7, 20, 29) (Discussion). Furthermore, the extended model accurately predicted the effect of a reduction of myosin concentration, suggesting that it is a fair representation of our experiments (SI Appendix, Fig. S2 A–F).

Using numerical simulations based on this model, we now could study how interactions among myosins would lead to actin sliding arrest. Simulations of very short actin filaments exhibited extended periods of global kinetic arrest of myosins (Fig. 2A). Simulations of intermediate length actin filaments exhibited alternating periods of kinetic arrest and kinetic activity of myosins (Fig. 2B). Simulations of long actin filaments did not exhibit periods of global kinetic arrest (Fig. 2C). However, local patches of prolonged binding of myosins to the actin filament did occur. When we measured the spatial extent of such arrest patches, we found that longer patches are generally less frequent than shorter patches (Fig. 2D). An exception are patches that span the entire length of the actin filament, which occur with an increased

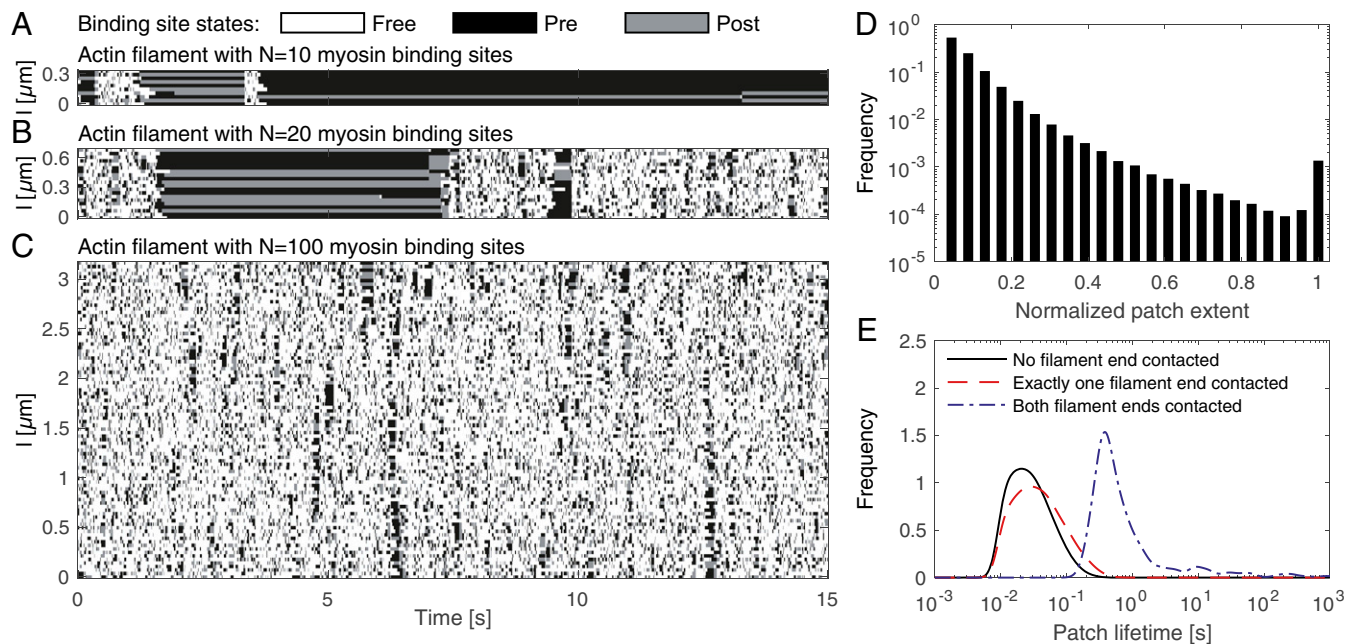


Fig. 2. Spontaneous kinetic arrest becomes long-term stable when it spreads to cover the entire actin filament. (A–C) Example evaluations of our detailed model with single myosin binding site resolution are shown for actin filaments of different length, $L = N \times 35.5$ nm (N refers to the number of myosin binding sites). Myosin binding site states are indicated by color, and their position along the actin filament (l) by the vertical axis. Note that binding sites always precede unidirectionally from the Free to the Pre, then to the Post, and then back to the Free state, even though states are not always visible due to finite time resolution in the display. Evaluations for all N exhibited 2 emergent states: 1) fast cycling through all 3 binding states, and 2) spatiotemporally contiguous domains of kinetic arrest, marked by Pre and Post state myosin binding sites, in agreement with previous work (8, 10). At low N , kinetic arrest dominates (A). At intermediate N , kinetic arrest and fast cycling alternate (B). At high N , kinetic arrest remains transient (C). (D) Histogram of the maximal spatial extent of individual arrest patches, normalized by total actin length L . In general, patches of larger extent are less frequent. This trend is inverted for patches that extend over the entire actin filament, which are again more frequent. Individual arrest patches were detected as temporally and spatially contiguous regions (connected components) of myosin-occupied binding sites. A single model evaluation over 10,000 s of an intermediate length filament ($N = 23$, or $L = 816.5$ nm) was analyzed so as to cover arrest as well as sliding phases. The model evaluation was resampled at 20-ms intervals for analysis; arrested patches that persisted for 100 ms or longer were included in the analysis. (E) Empirical probability distributions of patch lifetimes of patches that contact no end, one end, or both ends of the actin filament during their lifetime. (Same model evaluation as D, empirical probability distributions obtained by Gaussian kernel estimation with bandwidth 0.1, applied after \log_{10} transformation.)

frequency. We therefore hypothesized that the relatively short lifetime of arrest patches limits their longitudinal growth—except when the patches grow to the extent of covering the whole actin filament and become long-term stable. Indeed, when we analyzed the lifetimes of patches that reach none, one, or both ends of the actin filament, we found that prolonged kinetic arrest occurs only when patches reach both ends of the actin filament (Fig. 2E). This susceptibility toward persistent arrest at the filament ends can be understood as a consequence of the finite coupling length. An exponential decay of coupling with a decay length of 300 nm implies an equivalent of 8 myosin binding sites that are in reach from a filament end. In central regions of filaments longer than ≈ 600 nm, an equivalent of 16 binding sites is in reach. When comparing to previous work, 8 or 16 coupled binding sites correspond closely to conditions where myosin groups are persistently arrested or can transition into continuous kinetic activity, respectively (8). Taken together, our findings imply that the ends of actin filaments reduce the effective number of locally coupled myosin binding sites, so that kinetic arrest is stabilized when it reaches the filament ends. This scenario can explain why long-lived kinetic arrest is less likely for longer actin filaments, thus explaining the experimental observation that sliding arrest is less likely for longer actin filaments (8–10) (SI Appendix, Fig. S24).

Molecular Mechanics Can Be Mapped to a Generalized Spin Chain Model. To assess whether the conclusions that we made from our example system up to this point can be generalized to other

systems, we mapped our findings to a spin chain model (Fig. 3A). The spin chain model consists of N linearly ordered spins with nearest-neighbor connections. The spins can flip between 2 states ($s_{n=1,\dots,N} = \pm 1$). This model can be considered representative of the general class of finite, 1-dimensional systems with local coupling. The local coupling in our example system is included in the spin chain model in the form of a nearest-neighbor coupling with strength $\beta > 0$. The general bias toward activity exerted by myosin motors is represented by a global field $h > 0$ that acts on all spins. The stabilization of kinetic arrest at the filament ends is represented by a negative field with strength $h_0 > 0$ that is coupled only to the spins at the chain ends. A numerical evaluation of this model exhibited patches of inactivity, which could be compared to the arrest patches seen in our detailed mechanochemical model (Fig. 3B). As seen in the detailed simulation, sporadic and transient arrest occurred throughout the length of the chain. Also, patches of inactivity that contacted both chain ends were most persistent, while patches that contacted only 1 chain end persisted for shorter periods. One apparent difference occurs at the chain ends, where spins readily flip between activity and inactivity. While this is a difference in the microscopic kinetics of the spin chain model compared to the detailed molecular mechanics model, the global kinetics is preserved: The rapid flipping at the chain ends only changes into persistent inactivity when a patch of inactivity reaches the filament ends. Taken together, these results suggest that the spin chain model captures essential aspects of our detailed model. While the microscopic kinetics of spin chain ends differs from the detailed

actin filament (Fig. 4A) (13). We imagine, in principle, 2 opposing scenarios by which the length of actin could factor into this interaction. 1) As observed above, the kinetically active state that emerges from mechanical coupling of myosins is more robustly preserved for longer actin filaments. This implies that, for longer actin filaments, the actin-bound myosins are more likely to mount the forces required to resolve filamin cross-links. In this scenario, the sliding of longer actin should be less affected by filamin. 2) Since mechanical interactions are likely limited within a finite coupling range along the actin filament (*SI Appendix, Fig. S1*), filamin cross-links should then also be broken by forces mounted by myosins bound to actin within coupling range. In consequence, the mechanical interaction between cross-links and myosins can be seen as playing out within a local vicinity. Longer actin filaments would provide more space for such locally confined interactions, each of which has a chance to result in actin sliding arrest. In this scenario, the sliding of longer actin should be affected more strongly by filamin. In our experiments, filamin caused actin to be in the arrested state more frequently, while filamin did not reduce the velocity while actin is actually sliding (Fig. 4B and *SI Appendix, Fig. S4*). Our detailed model and our spin chain model reproduced this effect when we introduced cross-linkers that could bind anywhere along the actin filament (Fig. 4C). We therefore focused our further analysis on changes in f_{mot} . For low filamin concentrations ($[Fil] \lesssim 2.5$ nM), f_{mot} was reduced for all actin lengths but still exhibited an increase with actin length in agreement with scenario 1 (Fig. 5A). For higher

$[Fil]$, f_{mot} was also reduced for all actin lengths but decreased with actin length in agreement with scenario 2. We confirmed this second effect in a repeat experiment (*SI Appendix, Fig. S5*). Also, we found an increased autocorrelation time for intermediate $[Fil]$ (Fig. 5B). Taken together with the observation that the arrested and sliding state of actin remain distinct, the increased autocorrelation time suggests that the rate of switching between sliding and arrest was markedly reduced. Our detailed model and our spin chain model reproduced this effect when we introduced cross-linkers that could bind anywhere along the actin filament (Fig. 5C–F). Thus, at intermediate to high cross-linker concentrations, perturbations that result from cross-linker binding suppress activity more effectively for longer actin filaments.

Cross-Linkers Allow Patches of Arrested Myosins to Spread into Global Arrest Events. To explain how filamin might exert the observed effects on actin sliding, we investigated simulation results from both our models more closely. In the detailed model, binding of filamin appeared to be correlated with periods of sliding arrest (Fig. 6A). To investigate this apparent coordination, we extracted conditional return maps that were gated based on the binding of 1 filamin protein (Fig. 6B). These return maps revealed that, during periods when filamin is bound, the number of bound myosins increases to full occupation of the actin filament. With no filamin bound, the number of bound myosins decreases to a level typical of processive forward sliding of the actin filament. Hence, in the detailed model, the binding of a

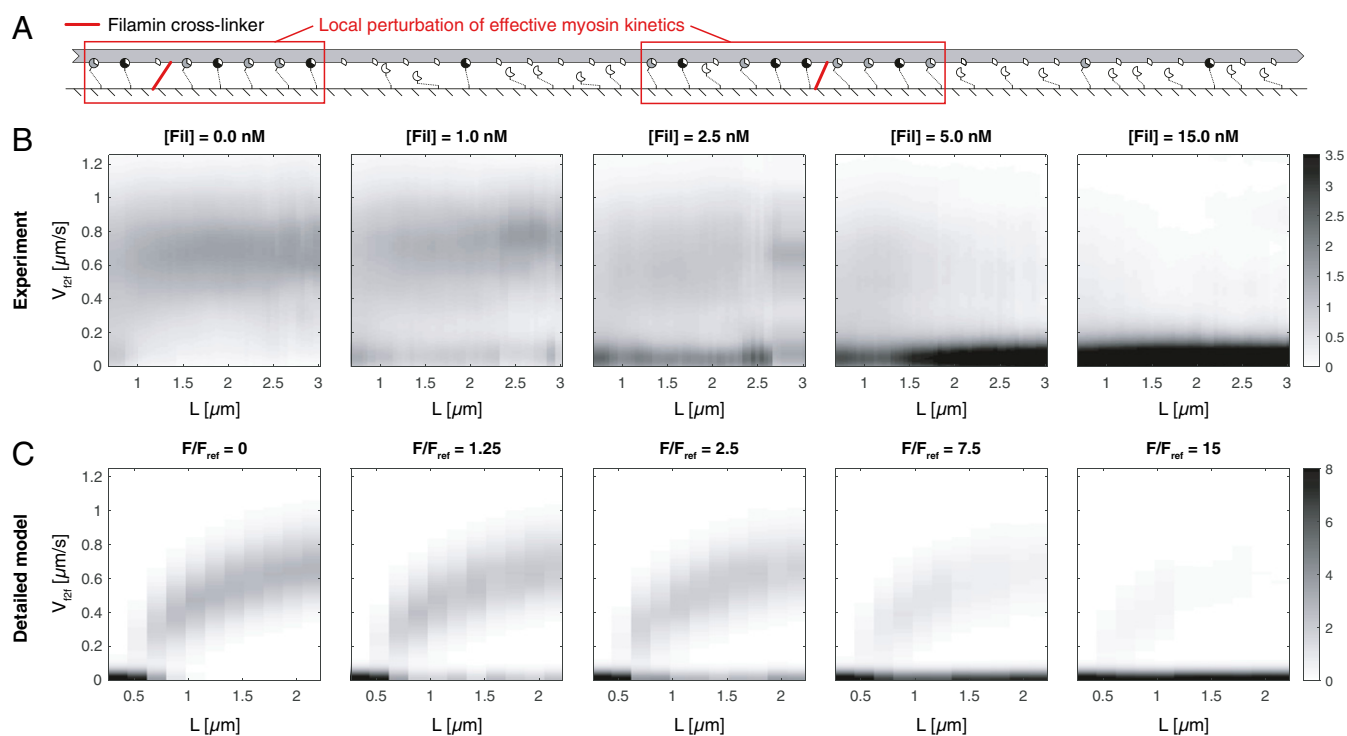


Fig. 4. Filamin biases actin into the arrested state but does not appreciably lower the velocity during periods of forward sliding. (A) To introduce external perturbations, we added the actin cross-linker filamin to our motility assay. Filamin attaches to actin and the motility surface, and is detached by mechanical stress exerted by close-by myosins (13). (B) Experimentally recorded actin sliding velocity distributions for increasing filamin concentrations ($[Fil]$). With increasing $[Fil]$, the probability to observe the active sliding state becomes less. The velocity of the sliding state is clearly distinguishable for all conditions except $[Fil] = 15.0$ nM, where no more sliding was visible. To create the displayed intensity images, actin filaments were binned by length (L); instantaneous velocities (frame-to-frame centroid displacements, V_{fzf}) were used to create empirical probability density distributions for a given L . The intensity of black coloring is proportional to the probability density. (C) Actin sliding velocities from simulations of the detailed model for increasing F , the average number of filamin proteins in binding range per myosin binding site. (F is rescaled with F_{ref} , the maximum F value used in the model evaluations, which resulted in a good fit to the $[Fil] = 15$ nM condition in our experiments; here, $F_{ref} = 0.06/15$). As seen in A, increasing F results in decreased probability to observe the active sliding state, while the sliding velocity is largely unaffected. Thirty-two model evaluations per L value; empirical probability densities were created from V_{fzf} values for simulations with a given number of binding sites N , which was converted into $L = N \cdot 0.0355 \mu\text{m}$.

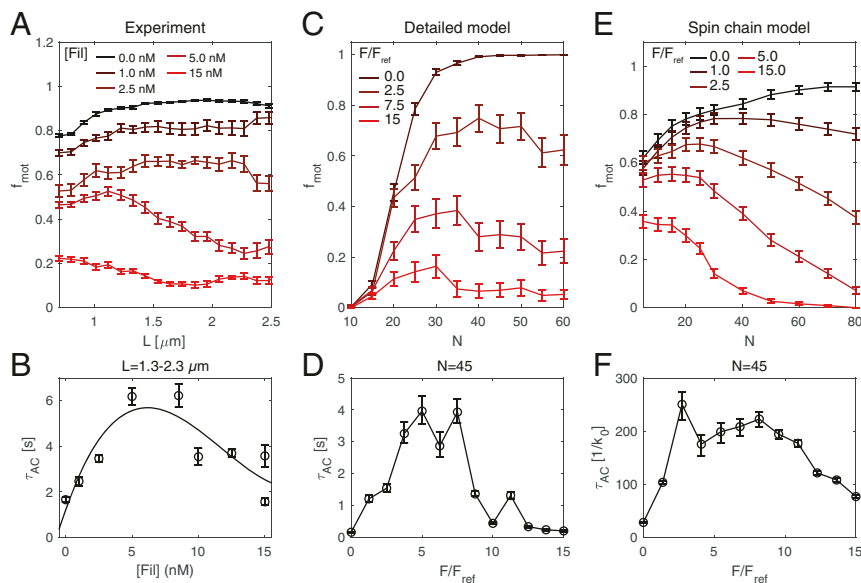


Fig. 5. Intermediate concentrations of the actin-surface cross-linker filamin more strongly arrest longer actin filaments. (A) Increasing filamin concentrations ([Fil]) progressively shut down actin sliding. For intermediate [Fil] (5.0 nM), filamin sliding was more effectively stopped at greater actin length (L). We confirmed this observation by a second set of experiments (SI Appendix, Fig. S5). The graph shows a running mean \pm SEM; $n = 6, 6, 7, 8,$ and 6 flow-through chambers per condition. Note that the analysis of f_{mot} across the displayed L range requires an analysis procedure that obscures the arrest at small L , as seen previously (8). (B) The sliding velocity autocorrelation time (τ_{AC}) for long actin filaments shows a transient increase for intermediate [Fil], indicating a slower switching between sliding and arrest in this experimental regime. The circles are mean \pm SEM; $n = 6, 6, 7, 8, 4, 4, 4, 4,$ and 6 flow-through chambers per condition (the data from the second set of experiments were included), Left to Right, Top to Bottom. A cubic polynomial was fitted to guide the eye (solid line). (C and D) The detailed model reproduced the experimentally observed dependence of f_{mot} and τ_{AC} on [Fil] and L (F as defined in Fig. 4C). All values are mean \pm SEM; $n = 32$ model evaluations per data point; same simulations as Fig. 4C. (E and F) The extended spin chain model equally reproduced the experimentally observed dependence of f_{mot} and τ_{AC} on [Fil] and L ($F_{ref} = 0.3/15$). Values are mean \pm SEM; $n = 200$ evaluations per data point.

single filamin to actin is sufficient to stabilize local patches of arrested myosins, which then spread and ultimately cover the entire actin filament. In the spin chain model with added cross-linkers, the binding of cross-linkers similarly allows the spreading of local patches of deactivated spins to cover the entire spin chain, in a manner comparable to the detailed model (SI Appendix, Fig. S6). Thus, both models suggest that the local perturbation by cross-linkers is relatively persistent and can sustain the spreading of patches of arrest into global arrest. Assuming a constant per-site likelihood of cross-linker binding, larger domains provide more opportunity for such perturbations to effect global kinetic arrest. Our experimental results demonstrate such a case, and our models provide a detailed explanation of the observed increase in actin sliding arrest with actin length.

Discussion

In this study, we found that local molecular mechanical perturbations impact the sliding of actin filaments differently depending on how these perturbations spread along the actin filament. Perturbations that stabilize only once they have spread throughout the entire filament are less likely to interfere with the sliding of longer filaments. Perturbations that are stable upon their occurrence and subsequently spread into global arrest are more likely to interfere with the sliding of longer filaments. This principle also applies to 1-dimensional, finite, and locally coupled systems in general, as demonstrated by our spin chain model.

To explain the sliding patterns of actin filaments that we observed in our experiments, we simulated the interaction of myosin and filamin with the actin filament at single-molecule resolution. Expanding on a previously developed model with single-molecule resolution (8), we here additionally considered the spatial distribution of protein attachment points along the actin filament. This extended model allowed us to explicitly account for the decay of the strength of mechanical coupling with

greater distance along the actin filament. In the previous model, which had no such spatial component, a saturation of the number of maximally coupled myosins had to be assumed ad hoc for long actin filaments (8). Our extended model inherently accounted for the saturation of actin sliding velocity when we included an exponential decay with a characteristic length of $0.3 \mu\text{m}$, and also when we included a linear decay with full loss of coupling at a length of $0.8 \mu\text{m}$. We interpret this as indication that the precise shape of the decay is not relevant to explain the observed saturation of actin sliding velocity, and that approximately one-half of the coupling strength is lost at a range of 300 to 400 nm. To compare this value to an independent estimate, we calculate the length l_{equ} at which the longitudinal stiffness of actin [$K_A = 43.7 \text{ pN/nm} \cdot (1/l_{equ})$] (29) is equal to the compound stiffness of a group of myosins that fully occupy a length of l_{equ} [$K_M = (l_{equ}/35.5 \text{ nm}) \cdot (2.5 \text{ pN/nm})$], assuming 1 taut myosin every 35.5 nm (7, 20). We interpret the resulting $l_{equ} \approx 130 \text{ nm}$ as a lower bound that supports the characteristic length estimate obtained by fitting our model. A previous estimate of $\approx 100 \mu\text{m}$ as the distance at which actin stiffness falls below myosin stiffness relied on a lower myosin stiffness (0.4 pN/nm), and did not consider that load-dependent detachment can lead to full myosin occupation of actin (23). Taken together, we have now obtained a physically credible, single-molecule level model of in vitro actin propulsion, which explicitly treats local mechanical interactions between proteins bound at different positions on the actin filament. Given that for myosin VI essentially the same length-dependent stop-and-go sliding behavior as seen in our study was observed, our model might be applicable also for other actin filament binding motors (25).

Upon evaluation of our extended model, we observed coordinated behavior of myosin and other proteins, which was spatially distributed along the actin filament. Specifically, we found that the spreading and shrinking of patches of kinetically arrested myosins play crucial roles in actin sliding and arrest. We are not aware

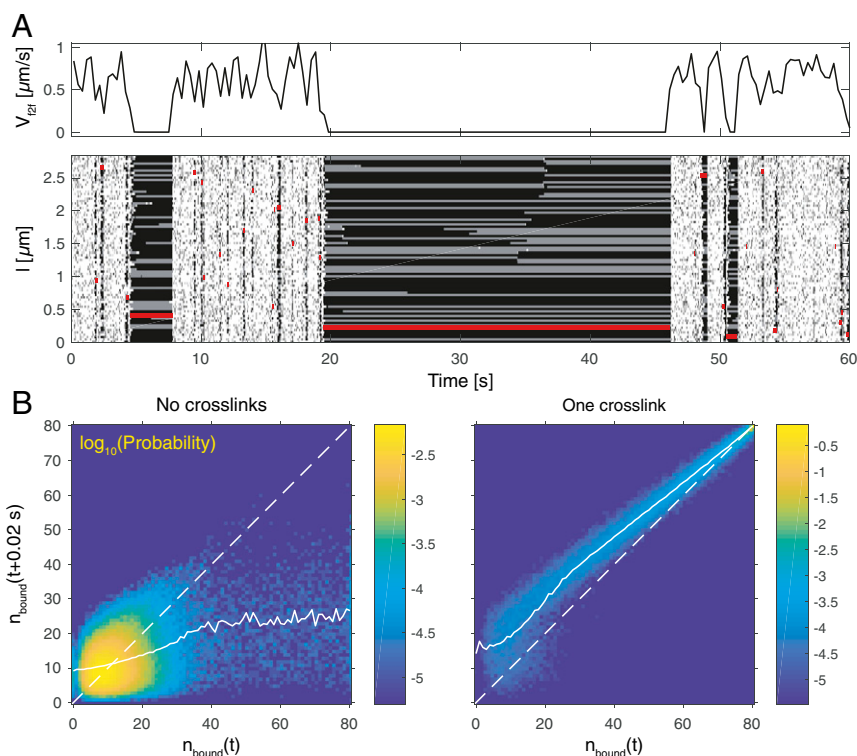


Fig. 6. Cross-linker binding allows patches of arrested myosins to spread into global arrest events. (A) A representative simulation of actin–myosin interaction in the presence of 1 filamin protein ($N=80$ myosin binding sites, corresponding to an actin length of $L=2.8045\ \mu\text{m}$, presence of only 1 filamin protein was assumed to prevent very long-lived actin sliding arrest events). The instantaneous sliding velocity (V_{fzk}) time course shows transitions between uninhibited sliding and arrest. The kymograph shows that myosin arrest and filamin binding (displayed in red) frequently occur at the same time. (B) Empirical return maps constructed from the number of bound myosins (n_{bound}) at a given time point t and with a delay of 0.02 s (pooled from 500 simulations of 200-s duration each). The average time evolution can be assessed by a comparison of the mean $n_{\text{bound}}(t+0.02\ \text{s})$ for a given $n_{\text{bound}}(t)$ (solid white line): Where the solid white line is above the $x=y$ diagonal (dashed white line), n_{bound} increases with time; where it is below, n_{bound} decreases with time. Points were added to the return maps selectively dependent on no filamin being bound (no cross-links) or 1 filamin being bound (1 cross-link) at $t+0.01\ \text{s}$; the color map represents the \log_{10} of the empirical probability.

of any existing experimental technique that could record such behavior from actual *in vitro* motility assays. Coming closest, the coordinated conformational changes of actin-regulatory proteins have been resolved in time and along the length of actin filaments by fluorescence microscopy (30, 31). While these experiments address a different aspect of molecular mechanics than our work, they also revealed patches of activation that initiate locally and then spread along the actin filament. Also, first experimental successes in tracking several motor proteins within the context of mechanically coupled groups have been reported (30). Both experimental advances indicate that the spatiotemporal coordination of molecular motor kinetics along actin filaments might be experimentally accessible in the future. The model evaluations we presented in this study provide clear, testable predictions for the dynamics of spreading and dissolution of patches of arrested myosins in such experiments.

We proposed an abstracted model consisting of a linear chain of spins, which reproduced key phenomena seen in the detailed model. This close correspondence suggests that the conclusions drawn from our experiments and the detailed model can be transferred to any other system that can be abstracted to the same type of spin chain model. This correspondence is therefore a crucial step in transitioning from observations in our particular example system to the generic class of finite, 1-dimensional systems. The success of such an abstraction can be seen in the example of processive transport motors and ribosomes, whose collective behavior could be classified as an asymmetric simple exclusion process (32, 33). The phenomena observed in our model

can be classified as conformational spread, a spatialized version of the classical Monod–Wyman–Changeux model, in our case with a linear geometry and nearest-neighbor coupling (34). Models of cooperativity in 1-dimensional geometries could also be applied to protein-binding motifs involved in gene regulation (35), especially considering the discovery of local neighborhoods of binding sites (36). Also, a close correspondence to the classical Zimm–Bragg model for the coil-to-helix transition in linear polymers exists (37). Specifically, the helix and the coil state correspond to the active and arrested state in our model, respectively. Besides differences in the role of ends of the linear chain, our model as well as the transfer matrix approach are identical. Furthermore, our findings closely correspond with more recent work in peptides (38). Experimentally, the lifetime of global helix conformations increases with peptide length (38). Theoretically, this length dependence was attributed to unfolding that initiates at the peptide ends and is less likely to spread to the center of longer peptides (38, 39). Also, modifications at the peptide ends can influence global outcomes, as found in our work (38). These correspondences strongly support our suspicion that our detailed model of actin propulsion maps to the generic class of linear spin chains. Such generic system classes allow one to neglect most details of underlying mechanisms. Instead, they capture emergent behaviors whose governing laws apply independently of underlying microscopic processes.

Methods Summary

Protein Purification and Preparation. Phasic smooth muscle myosin and actin were purified from tissue donations (Marvid Poultry, Montreal, QC, Canada), and prepared for motility assays as previously described (40–42). Purified

smooth muscle filamin A was generously provided by Apolinary Sobieszek, Institute for Biomedical Aging Research, Austrian Academy of Sciences, Vienna, Austria. Details are described in *SI Appendix*.

Motility Assay, Video Recording, and Analysis of Actin Sliding. Buffers, proteins, and flow-through chambers were prepared including several steps for the removal of catalytically defective myosin as previously described (8, 10). Concentrations of myosin and filamin were controlled by dilution in the initial myosin perfusion buffer and the final motility buffer, respectively. Videos of the sliding of fluorescent actin were recorded with a high numerical aperture objective and a CCD camera, and analyzed with our *ivma*³ software suite (available as open source) as previously described (9). The resulting frame-to-frame velocity (V_{f2f}) time traces with an effective time resolution of 0.33 s were used to calculate the mean actin sliding velocity (ν), the motile fraction (f_{mot} , fraction of frames with $V_{f2f} \geq 0.25 \mu\text{m/s}$), and the ensemble-corrected autocorrelation time (43, 44) (τ_{AC} ; *SI Appendix*, Fig. S7) for different actin lengths (L). Details are described in *SI Appendix*.

Detailed Model of Actin, Myosin, and Filamin Interaction. We simulated the mechanochemistry of individual myosin binding sites on a given actin filament as well as filamins cross-linking actin and the motility surface. To introduce the decay of mechanical coupling between proteins more distally placed along the actin filament, we rooted this mechanochemistry in local mechanical equilibria, evaluated from the location x of a given protein on the actin filament:

$$\sum_j \kappa(l_j - x) c_j (a - a_j^0) = 0.$$

$\kappa(\Delta x) = \exp(-|\Delta x|/L_c)$ represents a decay of mechanical coupling strength along the actin filament, with a characteristic length $L_c = 0.3 \mu\text{m}$. l_j indicates the attachment point of a given protein j on the actin filament; c_j , the stiffness; and a_j^0 , the linear sliding position of the actin filament at which the protein j is unstrained. The assumption of quasi-instantaneous mechanical equilibration is supported by previously measured longitudinal deformation response times of actin, which are well below 0.2 ms (29). Furthermore, consideration of only the linear sliding without viscous drag from the surrounding solvent is well justified in the motility assay as we prepared it (14). The local mechanical equilibrium is attained by adjusting the sliding position a of the actin filament. All reactions were assigned reaction rates without mechanical load, and reactions that included mechanical steps were additionally scaled by a prefactor $e^{-\Delta W^*}$. $\Delta W^* = W^* - W^{eq}$ is the mechanical work

required to reach the mechanically strained transition state (W^*) starting from the local mechanical equilibrium state (W^{eq}). The mechanical work levels W^* and W^{eq} can be calculated by applying the local mechanical equilibrium condition with and without the additional strain for the protein of interest to reach its transition state, respectively. The resulting rates were included in an extended Gillespie algorithm, to simulate actin sliding, which was sampled at time intervals $\Delta t = 0.33$ s as described previously (8, 10). Details are described in *SI Appendix*.

Spin Chain Model. We implemented a linear chain of spins, $\mathbf{s} = (s_1, s_2, \dots, s_N)$, where $s_n = \pm 1$. The spin chain potential energy was as follows:

$$H(\mathbf{s}) = - \sum_{n=1}^N s_i (h + \beta(s_{n-1} + s_{n+1})).$$

Here, $h > 0$ is an activating bias affecting all spins, and $\beta > 0$, the connection strength between nearest neighbors. The ends of the spin chain were padded by $s_0 = s_{N+1} = -h_0$, so that $h_0 > 0$ described a deactivating bias at the ends of the chain. From $H(\mathbf{s})$, the probability that all $s_n = 1$ could be exactly calculated to determine f_{mot} . Dynamics of the spin chain were analyzed using a Gillespie algorithm implementation, with transition rates $\exp(-(H(\mathbf{s}') - H(\mathbf{s})))$, where \mathbf{s}' indicates a proposed target configuration. The effect of cross-linkers was added by a second variable $c_n \in \{0, 1\}$, which monitors the binding of cross-linkers. Spins and cross-linkers influenced each other's kinetic rates, and their kinetics was also evaluated using the Gillespie algorithm. Details are described in *SI Appendix*.

ACKNOWLEDGMENTS. We acknowledge funding from the Helmholtz Program Biointerfaces in Technology and Medicine, the Max Planck Society, and the Natural Sciences and Engineering Research Council of Canada. The Meakins-Christie Laboratories (McGill University Health Centre) are supported in part by a center grant from Le Fonds de la Recherche en Santé du Québec. Z.B. was supported by the Costello Fund and a Master's Training Award from Le Fonds de la Recherche en Santé du Québec. L.H. was supported in part by an ELBE Postdoctoral Fellowship from the Center for Systems Biology Dresden. We thank Marvid Poultry for tissue donations; Apolinary Sobieszek for purified filamin; Pradeep Kumar Mohanty for discussing the spin chain model; Patrick McCall, Daniel Riveline, and the anonymous reviewers for constructive manuscript comments; Tyler Harmon, Alf Mansson, Thomas Quail, Sam Walcott, and Christoph Weber for discussions; and the Max Planck Institute for the Physics of Complex Systems for computing resources.

1. V. J. Anderson, H. N. W. Lekkerkerker, Insights into phase transition kinetics from colloid science. *Nature* **416**, 811–815 (2002).
2. T. Nagatani, The physics of traffic jams. *Rep. Prog. Phys.* **65**, 1331–1386 (2002).
3. T. Hägerstrand, Aspects of the spatial structure of social communication and the diffusion of information. *Pap. Reg. Sci.* **16**, 27–42 (1966).
4. T. C. Germann, K. Kadau, I. M. J. Longini Jr, C. A. Macken, Mitigation strategies for pandemic influenza in the United States. *Proc. Natl. Acad. Sci. U.S.A.* **103**, 5935–5940 (2006).
5. T. Quail, A. Shrier, L. Glass, Spatial symmetry breaking determines spiral wave chirality. *Phys. Rev. Lett.* **113**, 158101 (2014).
6. S. J. Kron, J. A. Spudich, Fluorescent actin filaments move on myosin fixed to a glass surface. *Proc. Natl. Acad. Sci. U.S.A.* **83**, 6272–6276 (1986).
7. W. Steffen, D. Smith, R. Simmons, J. Sleep, Mapping the actin filament with myosin. *Proc. Natl. Acad. Sci. U.S.A.* **98**, 14949–14954 (2001).
8. L. Hilbert, S. Cumarasamy, N. B. Zitouni, M. C. Mackey, A.-M. Lauzon, The kinetics of mechanically coupled myosins exhibit group size-dependent regimes. *Biophys. J.* **105**, 1466–1474 (2013).
9. L. Hilbert *et al.*, Molecular mechanical differences between isoforms of contractile actin in the presence of isoforms of smooth muscle tropomyosin. *PLoS Comput. Biol.* **9**, e1003273 (2013).
10. L. Hilbert, Z. Balassy, N. B. Zitouni, M. C. Mackey, A.-M. Lauzon, Phosphate and ADP differently inhibit coordinated smooth muscle myosin groups. *Biophys. J.* **108**, 622–631 (2015).
11. A. J. Ehrlicher, F. Nakamura, J. H. Hartwig, D. A. Weitz, T. P. Stossel, Mechanical strain in actin networks regulates FILGAP and integrin binding to filamin A. *Nature* **478**, 260–263 (2011).
12. K. Retailleau *et al.*, Arterial myogenic activation through smooth muscle filamin A. *Cell Rep.* **14**, 2050–2058 (2016).
13. J. M. Ferrer *et al.*, Measuring molecular rupture forces between single actin filaments and actin-binding proteins. *Proc. Natl. Acad. Sci. U.S.A.* **105**, 9221–9226 (2008).
14. T. Q. P. Uyeda, S. J. Kron, J. A. Spudich, Myosin step size. Estimation from slow sliding movement of actin over low densities of heavy meromyosin. *J. Mol. Biol.* **214**, 699–710 (1990).
15. J. E. Baker, C. Brosseau, P. Fagnant, D. M. Warshaw, The unique properties of tonic smooth muscle emerge from intrinsic as well as intermolecular behaviors of myosin molecules. *J. Biol. Chem.* **278**, 28533–28539 (2003).
16. J. E. Baker, C. Brosseau, P. B. Joel, D. M. Warshaw, The biochemical kinetics underlying actin movement generated by one and many skeletal muscle myosin molecules. *Biophys. J.* **82**, 2134–2147 (2002).
17. S. Walcott, D. M. Warshaw, E. P. Debold, Mechanical coupling between myosin molecules causes differences between ensemble and single-molecule measurements. *Biophys. J.* **103**, 501–510 (2012).
18. S. Walcott, The load dependence of rate constants. *J. Chem. Phys.* **128**, 215101 (2008).
19. P.-Y. Plaçais, M. Bolland, T. Guérin, J. F. Joanny, P. Martin, Spontaneous oscillations of a minimal actomyosin system under elastic loading. *Phys. Rev. Lett.* **103**, 158102 (2009).
20. M. Kaya, H. Higuchi, Nonlinear elasticity and an 8-nm working stroke of single myosin molecules in myofilaments. *Science* **329**, 686–689 (2010).
21. M. Kaya, Y. Tani, T. Washio, T. Hisada, H. Higuchi, Coordinated force generation of skeletal myosins in myofilaments through motor coupling. *Nat. Commun.* **8**, 16036 (2017).
22. F. Jülicher, J. Prost, Cooperative molecular motors. *Phys. Rev. Lett.* **75**, 2618–2621 (1995).
23. A. Vilfan, T. Duke, Instabilities in the transient response of muscle. *Biophys. J.* **85**, 818–827 (2003).
24. T. A. J. Duke, Molecular model of muscle contraction. *Proc. Natl. Acad. Sci. U.S.A.* **96**, 2770–2775 (1999).
25. R. F. Hariadi, A. J. Appukutty, S. Sivaramakrishnan, Engineering circular gliding of actin filaments along myosin-patterned DNA nanotube rings to study long-term actin-myosin behavior. *ACS Nano* **10**, 8281–8288 (2016).
26. C. Veigel, J. E. Molloy, S. Schmitz, J. Kendrick-Jones, Load-dependent kinetics of force production by smooth muscle myosin measured with optical tweezers. *Nat. Cell Biol.* **5**, 980–986 (2003).
27. M. Capitanio *et al.*, Two independent mechanical events in the interaction cycle of skeletal muscle myosin with actin. *Proc. Natl. Acad. Sci. U.S.A.* **103**, 87–92 (2006).
28. M. Capitanio *et al.*, Ultrafast force-clamp spectroscopy of single molecules reveals load dependence of myosin working stroke. *Nat. Methods* **9**, 1013–1019 (2012).
29. H. Kojima, A. Ishijima, T. Yanagida, Direct measurement of stiffness of single actin filaments with and without tropomyosin by in vitro nanomanipulation. *Proc. Natl. Acad. Sci. U.S.A.* **91**, 12962–12966 (1994).
30. R. Desai, M. A. Geeves, N. M. Kad, Using fluorescent myosin to directly visualize cooperative activation of thin filaments. *J. Biol. Chem.* **290**, 1915–1925 (2015).
31. S. Walcott, N. M. Kad, Direct measurements of local coupling between myosin molecules are consistent with a model of muscle activation. *PLoS Comput. Biol.* **11**, e1004599 (2015).

32. S. Klumpp, R. Lipowsky, Traffic of molecular motors through tube-like compartments. *J. Stat. Phys.* **113**, 233–268 (2003).
33. C. T. MacDonald, J. H. Gibbs, A. C. Pipkin, Kinetics of biopolymerization on nucleic acid templates. *Biopolymers* **6**, 1–5 (1968).
34. D. Bray, T. Duke, Conformational spread: The propagation of allosteric states in large multiprotein complexes. *Annu. Rev. Biophys. Biomol. Struct.* **33**, 53–73 (2004).
35. L. Bintu *et al.*, Transcriptional regulation by the numbers: Models. *Curr. Opin. Genet. Dev.* **15**, 116–124 (2005).
36. W. A. Whyte *et al.*, Master transcription factors and mediator establish super-enhancers at key cell identity genes. *Cell* **153**, 307–319 (2013).
37. B. H. Zimm, J. K. Bragg, Theory of the phase transition between helix and random coil in polypeptide chains. *J. Chem. Phys.* **31**, 526–535 (1959).
38. S. Neumaier, A. Reiner, M. Büttner, B. Fierz, T. Kiefhaber, Testing the diffusing boundary model for the helix-coil transition in peptides. *Proc. Natl. Acad. Sci. U.S.A.* **110**, 12905–12910 (2013).
39. B. Fierz, A. Reiner, T. Kiefhaber, Local conformational dynamics in α -helices measured by fast triplet transfer. *Proc. Natl. Acad. Sci. U.S.A.* **106**, 1057–1062 (2009).
40. A. Sobieszek, “Smooth muscle myosin: Molecule conformation, filament assembly and associated regulatory enzymes” in *Airways Smooth Muscle: Biochemical Control of Contraction and Relaxation*, D. Raeburn, M. A. Giembycz, Eds. (Respiratory Pharmacology and Pharmacotherapy, Birkhäuser, 1994).
41. J. D. Pardee, J. A. Spudich, Purification of muscle actin. *Methods Enzymol.* **85**, 164–181 (1982).
42. D. M. Warshaw, J. M. Desrosiers, S. S. Work, K. M. Trybus, Smooth muscle myosin cross-bridge interactions modulate actin filament sliding velocity in vitro. *J. Cell Biol.* **111**, 453–463 (1990).
43. K. E. Trenberth, Some effects of finite sample size and persistence on meteorological statistics. Part I: Autocorrelations. *Mon. Weather Rev.* **112**, 2359–2368 (1984).
44. A. Menzel, E. H. Conrad, M. C. Tringides, M. Kammler, M. Horn von Högen, Finite collection time effects in autocovariance function measurements. *J. Appl. Phys.* **93**, 2229–2235 (2003).